Differential Effects of Alkyl- and Arylguanidines on the Stability and Reactivity of Inducible NOS Heme−Dioxygen Complexes[†]

Magali Moreau,[‡] Jean-Luc Boucher,*,[‡] Tony A. Mattioli,[§] Dennis J. Stuehr,[||] Daniel Mansuy,[‡] and Jérôme Santolini[§]

Laboratoire de Chimie et Biochimie Pharmacologiques et Toxicologiques, UMR 8601 CNRS, Université Paris V R. Descartes, 45 Rue des Saints-Pères, 75270 Paris Cedex 06, France, Laboratoire de Biophysique du Stress Oxydant, DBJC-SBE, CEA-Saclay, 91191 Gif sur Yvette, France, and Department of Immunology, The Lerner Research Institute, Cleveland Clinic Foundation, 9520 Euclid Avenue, Cleveland, Ohio 44195

ABSTRACT: NO-Synthases are heme proteins that catalyze the oxidation of L-arginine into NO and L-citrulline. Some non-amino acid alkylguanidines may serve as substrates of inducible NOS (iNOS), while no $NO^{\bullet}$ production is obtained from arylguanidines. All studied guanidines induce uncoupling between electrons transferred from the reductase domain and those required for NO formation. This uncoupling becomes critical with arylguanidines, leading to the exclusive formation of superoxide anion $O_2^{\bullet-}$ as well as hydrogen peroxide H_2O_2. To understand these different behaviors, we have conducted rapid scanning stopped-flow experiments with dihydrobiopterin (BH_2) and tetrahydrobiopterin (BH_4) to study, respectively, the (i) autoxidation and (ii) activation processes of heme ferrous−O_2 complexes ($Fe^{II}O_2$) in the presence of eight alkyl- and arylguanidines. The $Fe^{II}O_2$ complex is more easily autooxidized by alkylguanidines (10-fold) and arylguanidines (100-fold) compared to L-arginine. In the presence of alkylguanidines and BH_4, the oxygen-activation kinetics are very similar to those observed with L-arginine. Conversely, in the presence of arylguanidines, no $Fe^{II}O_2$ intermediate is detected. To understand such variations in reactivity and stability of $Fe^{II}O_2$ complex, we have characterized the effects of alkyl- and arylguanidines on $Fe^{II}O_2$ structure using the $Fe^{II}CO$ complex as a mimic. Resonance Raman and FTIR spectroscopies show that the two classes of guanidine derivatives induce different polar effects on $Fe^{II}CO$ environment. Our data suggest that the structure of the substituted guanidine can modulate the stability and the reactivity of heme−dioxygen complexes. We thus propose differential mechanisms for the electron- and proton-transfer steps in the NOS-dependent, oxygen-activation process, contingent upon whether alkyl- or arylguanidines are bound.

Nitric oxide (NO)[1] is an ubiquitous molecule that plays key roles in a variety of physiological processes in mammals such as neurotransmission, vasorelaxation, platelet aggregation, and immune responses (*1*). In mammals, NO is synthesized by heme proteins, NO synthases (NOSs), that catalyze a two-step oxidation of L-arginine with intermediate formation of N^{ω}-hydroxy-L-arginine (NOHA) (eq 1) (*2*).

Various pathological processes are related with either overproduction of NO (migraine and septic shock) or deficit in NO production (atherosclerosis and hypertension) (*3*, *4*). Therefore, NOSs constitute interesting targets for drug design (*5*, *6*), and many studies are undertaken to better understand the mechanism of NO-synthesis catalyzed by NOSs (*2*, *7−11*).

$$RNH\text{-}C(=NH)\text{-}NH_2 \xrightarrow[O_2 \quad H_2O]{1\ NADPH} RNH\text{-}C(=NOH)\text{-}NH_2 \xrightarrow[O_2 \quad H_2O]{0.5\ NADPH} RNH\text{-}C(=O)\text{-}NH_2 + NO^{\circ}$$

L-arginine N^{ω}-hydroxy-L-arginine,   L-citrulline
                              NOHA

$R = NH_2\text{-}CH(CO_2H)\text{-}(CH_2)_3\text{-}$

There are three isoforms of NOS: neuronal NOS (nNOS), endothelial NOS (eNOS), and inducible NOS (iNOS). All of them are active in their homodimeric form consisting of an NH_2-terminal oxygenase domain that contains binding sites for the heme prosthetic group, substrate L-arginine, and cofactor (6R)-5,6,7,8-tetrahydro-L-biopterin (BH_4). The CO_2H-terminal reductase domain contains binding sites for flavins FMN and FAD as well as NADPH and displays strong similarities with cytochrome P450 reductase (*12*). These two domains are fused by a Ca^{2+}-dependent calmodulin (CaM)-binding domain. CaM binding triggers an electron flow from the reductase domain to the heme domain (*2*, *3*, *10*, *13*).
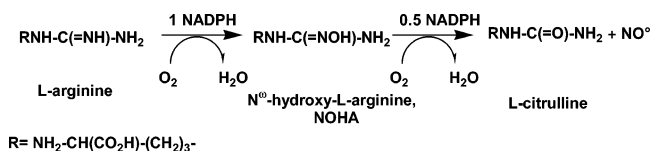
* Corresponding author. Tel: 33 1 42 86 21 91. Fax: 33 1 42 86 83 87. E-mail: jean-luc.boucher@univ-paris5.fr.
[‡] Université Paris V R. Descartes.
[§] DBJC-SBE.
[||] Cleveland Clinic Foundation.

[1] Abbreviations: ATR−FTIR, attenuated total reflection−Fourier transformed infrared spectroscopy; BH_4, tetrahydrobiopterin; BH_2, dihydrobiopterin; CaM, calmodulin; $CF_3(CH_2)_3$guanidine, 4,4,4-trifluorobutylguanidine; DTT, dithiothreitol; $Fe^{II}O_2$, ferrous heme dioxygen complex; $Fe^{II}CO$, ferrous heme carbon monoxide complex; fwhm, full width at half-maximum; n, i, and eNOS, neuronal, inducible, and endothelial NOS; iNOSoxy, oxygenase domain of iNOS; NOHA, N^{ω}-hydroxy-L-arginine; NO, nitric oxide; RR, resonance Raman spectroscopy; NOS, nitric oxide synthase; 2-Fphguanidine, 2-fluorophenylguanidine hydrochloride; 4-Fphguanidine, 4-fluorophenylguanidine hydrochloride; 4-Clphguanidine, 4-chlorophenylguanidine hydrochloride; 4-MeOphguanidine, 4-methoxyphenylguanidine hydrochloride.

The latest proposed mechanism for the first step of L-arginine oxidation consists of the following steps: The first electron is brought by the reductase domain to reduce the resting ferric (Fe^{III}) enzyme to a ferrous (Fe^{II}) state (*2, 10*). Then, oxygen binding leads to a ferrous–dioxygen complex ($Fe^{II}O_2$) (*14*). Recent mechanistic studies propose that BH_4 transfers the second electron and a concomitant proton resulting in the buildup of ferric hydroperoxo complex (Fe^{III}–OOH) (*15–22*). By analogy with the P450 monooxygenation mechanism, the Fe^{III}–OOH intermediate, after protonation and through heterolytic cleavage of the O–O bond, leads to the reactive oxoferryl $Fe^{IV}(=O)$ porphyrin π-cation radical (*23, 24*). This last species would be able to hydroxylate the guanidine moiety of L-arginine. NOSs show high substrate specificity: only the amino acids homo-L-arginine or homo-L-NOHA were found to be substrates of NOS (*25, 26*). However, NOSs have been shown to catalyze NO formation by oxidation of some non-amino acid alkyl- and arylhydroxyguanidines following reactions similar to the oxidations of natural substrates, L-arginine and NOHA (*6, 27–30*). Hydroxyguanidine-based compounds are not very stable and are highly sensitive to chemical or peroxidase-catalyzed oxidations, which make them unsuitable for pharmaceutical applications (*31, 32*). In this respect, guanidine derivatives are more stable and seem more attractive as new NO precursors, and we showed that some simple substituted guanidines could lead to NO• synthesis by NOS (*33*). Nonetheless, the oxidation of the guanidine moiety seems to be much more difficult since fewer guanidine than hydroxyguanidine derivatives were found to be substrates of NOSs (*6, 28–30*). We showed that iNOS was able to catalyze the oxidation of some alkylguanidines, such as 4,4,4-trifluorobutylguanidine **2** ($CF_3(CH_2)_3$guanidine), into NO with activity up to 40% relative to L-arginine (*33*). Conversely, all the tested arylguanidines failed to produce NO from incubations with full-length iNOS containing all its cofactors (*28–30, 33*).

Production of NO from L-arginine requires 1.5 NADPH equiv, that is, three electrons (eq 1). The determination of the stoichiometry of multiturnover reactions with iNOS in the presence of the non-amino acid guanidine derivatives showed that the alkylguanidine substrates increased the electron flow transferred from the reductase domain, resulting in an uncoupling of electrons furnished by NADPH compared to electrons necessary to form NO. For example, in full-length iNOS, $CF_3(CH_2)_3$guanidine led to a ratio of oxidized NADPH to NO produced of around 3:1 (*33*). The arylguanidines showed an even higher NADPH consumption without any detection of NO and urea, but high amounts of H_2O_2 and $O_2^{•-}$ were produced (to be published).

To understand why the arylguanidines failed to produce NO whereas some alkylguanidines could be NO precursors (*28–30, 33*), we investigated whether these guanidine-based compounds could influence the ferrous–dioxygen complex ($Fe^{II}O_2$) stability and the first steps of oxygen activation in iNOSoxy. Autoxidation of the $Fe^{II}O_2$ complex can lead to Fe^{III} and $O_2^{•-}$ release and electron uncoupling (*34–36*). Oxygen activation steps are thus critical for the formation of $Fe^{IV}(=O)$ and, therefore, for NOS ability to efficiently oxidize guanidine derivatives into NO.

To study heme $Fe^{II}O_2$ stability, we evaluated the autoxidation rates of $Fe^{II}O_2$ by rapid-mixing stopped-flow spectroscopy after mixing O_2 and ferrous iNOSoxy saturated with various guanidines and in the presence of BH_2, an analogue of BH_4 that does not activate $Fe^{II}O_2$ (*17, 37*). The same experiments performed in the presence of BH_4 allowed us to study the oxygen activation processes. Both alkyl- and arylguanidines allowed $Fe^{II}O_2$ formation, but its stability and reactivity seem to strongly depend on the nature of the guanidine bound to the active site. We checked whether these differences could arise from direct effects of the guanidines on $Fe^{II}O_2$ structure. Ferrous heme–CO ($Fe^{II}CO$) was thus used as a probe for evaluating the influence of alkyl- and arylguanidines on heme environment, and we studied Fe^{II}-CO vibration modes by resonance Raman (RR) and Fourier transformed infrared (FTIR) spectroscopy. All the collected data showed specific effects of alkyl- and arylguanidines on $Fe^{II}CO$ structure and allowed us to propose different mechanisms for oxygen activation in the presence of alkyl- or arylguanidines.

MATERIALS AND METHODS

Chemicals. BH_4 and BH_2 were obtained from Schircks Laboratory (Jona, Switzerland). Chemicals and reagents of the highest grade commercially available were obtained from Aldrich, Fluka, or Janssen. The synthesis and physicochemical characteristics of the hydrochloride salts of agmatine **1**, 4,4,4-trifluorobutylguanidine **2**, *n*-pentylguanidine (Pentylguanidine) **3**, 4-fluorophenylguanidine (4-Fphguanidine) **5**, 4-chlorophenylguanidine (4-Clphguanidine) **6**, and 4-methoxyphenylguanidine (4-MeOphguanidine) **7** have been described elsewhere (*33*). 2-Fluorophenylguanidine hydrochloride (2-Fphguanidine) **4** has been synthesized from 2-fluoroaniline and *N*-*N*′-bis(*tert*-butyloxycarbonyl)pyrazol carboxamidine following a general procedure for the preparation of guanidines (*38*).

Enzyme Preparation. Mouse iNOS oxygenase domain (iNOSoxy) containing a six-histidine tag at its C-terminus was expressed in *Escherichia coli* BL21 using the PCWori vector and purified as already described (*39*) in the absence of BH_4 and L-arginine. This oxygenase domain displayed all the spectroscopic properties of the full-length enzyme and its His_6-tag did not modify its reactivity (*39*). Its concentration was determined from the absorbance at 444 nm of the heme $Fe^{II}CO$ complex using an extinction coefficient of 76 $mM^{-1}\cdot cm^{-1}$ (*40*).

Stopped-Flow Experiments. The protein samples containing BH_4 were obtained by preincubation at 4 °C for 1 h in the presence of 100 μM BH_4, 3 mM DTT, and 10 mM L-arginine or 30 mM of compounds **1–7** in 50 mM HEPES buffer (pH 7.4). The binding of the guanidine derivatives and BH_4 was confirmed by measuring the low-spin (420 nm) to the high-spin (395 nm) transition of the heme using UV–vis spectroscopy (*37*). The protein samples containing BH_2 were preincubated overnight at 4 °C with 250 μM BH_2, 2.5 mM DTT, and 10 mM L-arginine or 30 mM of compounds **1–7** in the same buffer. The samples were made anaerobic by several cycles of vacuum and argon refilling. The reduction of the heme was achieved by progressive addition of an anaerobic solution of sodium dithionite and followed by monitoring the change of the Soret peak from 395 nm for the ferric form to 412 nm for the ferrous one (*17, 22, 41, 42*). The rapid-mixing stopped-flow experiments were

performed at 10 °C on a Bio-Logic SFM 300 instrument customized for anaerobic and semianaerobic experiments and connected to a Tidas 1024-diode array detector able of recording spectra every 3 ms. The reduced enzyme was transferred into the stopped-flow apparatus with a gastight syringe and was rapidly mixed with an equal volume of air-saturated buffer. Spectra were recorded between 300 and 700 nm with the following sequence: first, 250 spectra every 3 ms, then 250 spectra every 9 ms, and, finally, 250 spectra every 18 ms, for a total measurement time of 7.5 s.

Stopped-Flow Data Analysis. Different approaches have been used in previous papers to analyze the data of heme transitions occurring in the first steps of the catalysis (*14*, *17*, *21*, *22*, *41*, *42*). To get results as accurate as possible, we used two different methods: (i) a direct examination of the recorded spectra with exponential fittings of the absorbance cross sections at specific wavelengths performed with OriginPro 7.5 software (OriginLab Corporation, Northampton, MA) and (ii) a global analysis of the heme transition with the software SPECFIT/32 v3.0 37 (Spectrum Software associates, Marlborough, MA) that fitted series of 3D data obtained from multiwavelength measurements to a predetermined kinetic model. First, visual analysis of the spectra with OriginPro allowed us to identify the different heme species involved in the single turnover reaction: ferrous Fe^{II} (~412 nm), ferrous dioxygen $Fe^{II}O_2$ (427−430 nm), and ferric Fe^{III} (395 nm) complexes. The presence of isobestic points confirmed the monophasic transitions between the different species. This allowed the determination of quantitative transition rates that were obtained by fitting to monoexponential functions the absorbance cross sections at wavelengths corresponding to $Fe^{II}O_2$ decay (427 nm) and to ferric iNOSoxy recovery (395 and 650 nm). The SPECFIT global analysis enabled us to perform single value decomposition of the recorded spectra based on different mechanistic models. For most experiments, a "A → B → C" model best fit the data; when not possible, a "A → B" model was chosen. This analysis provided us with the calculated spectra for the different species A, B, and C and with the kinetic rates of the transitions between them. For data analysis of the experiments conducted with BH_2, the rates estimated by the global analysis matched the ones obtained by direct fitting at specific wavelengths. In the presence of BH_4, calculated parameters were slightly different (Table 2). The discrepancy between the two methods might arise from the fact that the first transition $Fe^{II} → Fe^{II}O_2$ is so fast that the very first spectrum consists of a mixture of Fe^{II} and $Fe^{II}O_2$. This made more difficult for SPECFIT to accurately distinguish the first spectra and the rates of the following transitions. Nevertheless, both methods lead to very similar kinetics rates.

Resonance Raman Spectra. Samples for the RR experiments were prepared in 0.1 M potassium phosphate buffer (pH 7.4) with different combinations of L-arginine (100 μM) or substituted guanidines **1**−**7** (10 mM), BH_4 (400 μM), and DTT (3 mM). Samples were washed by two successive cycles of dilution/centrifugation in this final buffer using a Millipore membrane filter (30 kDa cutoff). The binding of the compounds and BH_4 was again confirmed by the spin state changes of the ferric heme followed by UV−vis spectroscopy. Enzyme concentrations for RR studies ranged between 150 and 200 μM. Forty microliters of the anaerobic Fe^{III} iNOSoxy was prepared directly in quartz EPR tubes

sealed with airtight rubber septa after 60 cycles of alternate vacuum and argon refilling. Ferrous samples were obtained by reduction of Fe^{III} iNOSoxy with addition of a small volume of dithionite solution (final concentration of ~5−10 mM) directly into the EPR tube using a gastight syringe (Hamilton). Ferrous heme−CO samples were obtained by flushing CO inside the EPR tube for 10 min to ensure complete CO saturation of the solution. The samples were placed into a gastight quartz spinning cell to avoid local heating and to prevent photodissociation and degradation of the NOS samples. Excitation at 441.6 nm was obtained with a He−Cd laser (Kimmon). Resonance Raman spectra were recorded at room temperature using a modified single-stage spectrometer (Jobin-Yvon T64000) equipped with a liquid N_2-cooled back-thinned CCD detector. Stray scattered light was rejected using a holographic notch filter (Kaiser Optical Systems). Spectra were recorded by the co-addition of 40−240 individual spectra with an exposure time of 10−20 s each (total accumulation time between 20 and 60 min for each spectral window). Three to six successive sets of such spectra were then averaged. Laser power on the sample was kept below 5 mW to avoid photodissociation and photooxidation (*43*, *44*). To accurately determine small frequency differences, the monochromator was calibrated using the excitation wavelength, and samples to be directly compared were recorded the same day with the same optical geometry. Spectral precision and accuracy were estimated to be ±1 cm^{-1}. Baseline corrections were performed using GRAMS 32 software (Galactic Industries, Salem, NH). The iNOSoxy RR bands were assigned following previous publications on iNOS and other NOSs (*43*, *45*−*47*).

ATR−FTIR Experiments. iNOSoxy $Fe^{II}CO$ complexes were prepared as described for the RR experiments, and protein samples were concentrated up to around 600 μM. Oxygen removal was achieved in a sealed cuvette by 3 × 20 cycles of alternate vacuum and argon refilling. Small volumes of dithionite solution were added to reach a final dithionite concentration around 15 mM. $Fe^{II}CO$ complexes were then obtained by 5 min of CO flushing inside the cuvette. FTIR spectra were recorded using Bruker IFS 66/S Fourier transform infrared spectrometer coupled to a single reflection micro ATR unit from Pike technologies. Ten microliters of an iNOSoxy $Fe^{II}CO$ sample was placed on the ZnSe crystal surface of the ATR unit. The device was sealed with a gastight in-house-built chamber and maintained under a flush of CO for 15 min until the sample was sufficiently dry. Twenty to thirty co-added interferograms were averaged for each spectrum. In some cases, a water vapor spectrum was used for background correction. Baseline correction was achieved using the GRAMS 32 software package. Each curve corresponded to the average of two to three individual experiments. Band peaks were identified using 2nd-derivative analysis (GRAMS 32). These frequencies were used in a re-iterative Lorentzian band fitting routine to fit crowded spectral region.

RESULTS

Influence of Alkyl- and Arylguanidines on Autoxidation Rates of $Fe^{II}O_2$. $Fe^{II}O_2$ buildup and stability were investigated by rapid-mixing of anaerobic ferrous iNOSoxy solution containing BH_2 and various substituted guanidines with an air-saturated buffer. Spectral changes were analyzed by rapid-
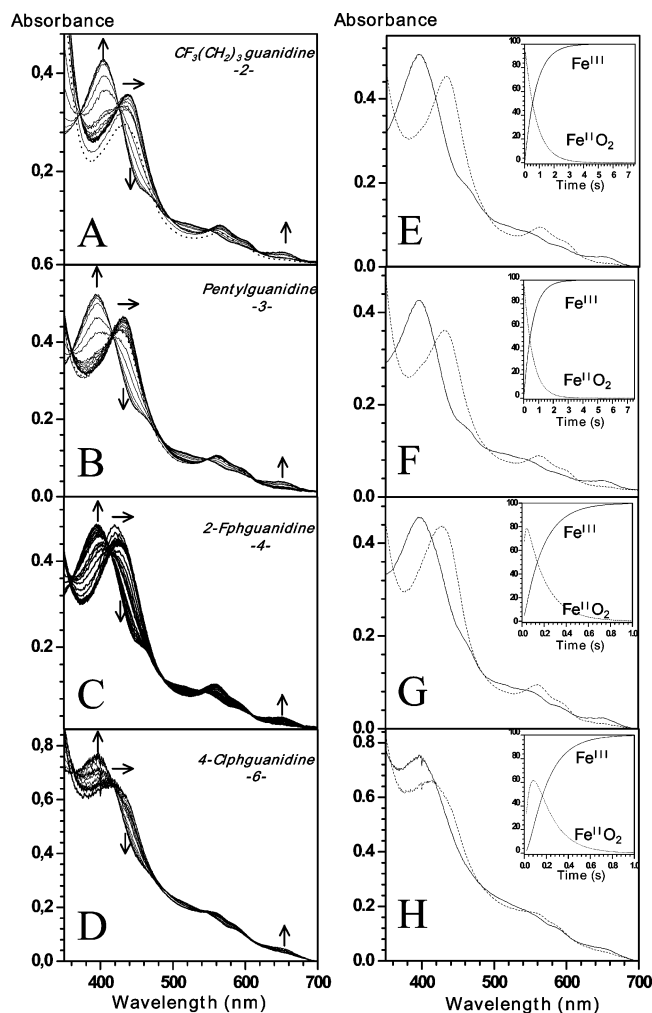
FIGURE 1: Heme transitions in single-turnover reaction of BH$_2$-saturated iNOSoxy with O$_2$ in the presence of alkyl- and arylguanidines. Ferrous iNOSoxy saturated with BH$_2$ was rapidly mixed at 10 °C with air-saturated buffer. Panels A−D show the superimposed spectra recorded in the presence of CF$_3$(CH$_2$)$_3$-guanidine **2**, pentylguanidine **3**, 2-Fphguanidine **4**, and 4-Clphguanidine **6**, respectively. Panels E−F display the spectra of Fe^{II}O$_2$ and Fe^{III} in the presence of compounds **2**, **3**, **4**, and **6** calculated by global analysis with SPECFIT/32. The insets display the resulting heme transition kinetics reported as percentage of the total heme transition.

scanning UV/visible absorption spectrometry with spectra recorded every 3, 6, and then 18 ms for an overall kinetics of 7.5 s. Figure 1A,B shows the superimposed spectra obtained for two representative alkylguanidines **2** and **3**. We were able to distinguish similar spectral species for all the studied alkylguanidines: first few spectra showed a species absorbing at 425−426 nm followed by an intermediate species with maximal absorption at ∼430 nm and two broad bands at 560−565 and 595−600 nm, corresponding to the Fe^{II}O$_2$ complex, and finally the recovery of the ferric iNOSoxy at 395 nm (*14, 17, 21, 48, 49*). The first recorded spectra with a Soret maximum at 425−426 nm should correspond to a mixture of the initial Fe^{II} (412 nm) and the intermediate Fe^{II}O$_2$ (430 nm). Oxygen binding on heme Fe^{II} species was too fast to be accurately monitored by our diode array detector, and the rate of formation of Fe^{II}O$_2$ in the presence of BH$_2$ and any of the alkylguanidines was estimated to be very fast ($k > 50$ s^{-1}) (*41, 50*). The presence of well-defined isosbestic points showed the successive

conversion of one species into the other. The fitting of the absorbance cross sections at 427 nm (Fe^{II}O$_2$ decay) and at 395 and 650 nm (high-spin heme Fe^{III} recovery) gave apparent rate constants ranging from 1.6 to 1.9 s^{-1} for the Fe^{II}O$_2 \rightarrow$ Fe^{III} transition (Table 1), around 10 times faster than the rate reported in the presence of L-arginine (0.2 s^{-1}, Table 1) (*17*).
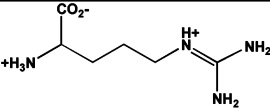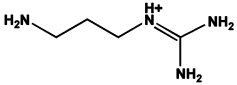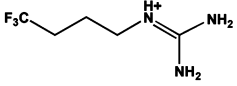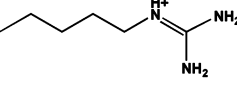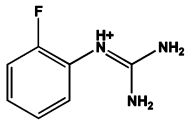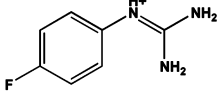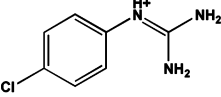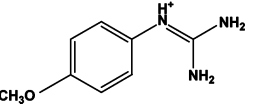
The single value decomposition analysis of the spectra was best fitted to a common "A → B → C" model with two monophasic transitions. Figure 1E,F shows the calculated spectra of heme Fe^{II}O$_2$ (430 nm) and Fe^{III} (395 nm) in the presence of alkylguanidines **2** and **3**. The kinetics of the Fe^{II}O$_2 \rightarrow$ Fe^{III} transition are displayed in the insets of Figure 1E,F. The calculated rate constants, 0.4 s^{-1} for agmatine **1** and 1.6−1.9 s^{-1} for the other alkylguanidines **2** and **3**, exactly matched those obtained by direct fitting at different wavelengths (Table 1).

The same experiments have been conducted with the arylguanidines **4**−**7**. Figure 1C,D shows the superimposed spectra recorded for iNOSoxy with BH$_2$ and the arylguanidines **4** and **6**. For all arylguanidines, absorption maxima were found at 420−422 nm for the first spectra, then between 425 and 427 nm for the intermediate Fe^{II}O$_2$, and at 395 nm for the final Fe^{III}. Again, we could estimate Fe^{II}O$_2$ buildup rate to exceed 50 s^{-1}. Kinetics were fitted at the same multiple wavelengths used for alkylguanidines, and Fe^{II}O$_2$ decay rates varied between 7 and 19 s^{-1} (Table 1). The global analysis best fitted the data to the same "A → B → C" model. Figure 1G,H shows the calculated spectra of Fe^{II}O$_2$ (427 nm) and Fe^{III} (396 nm) and, in insets, the transition kinetics for arylguanidines **4** and **6**. The global analysis and the fitting at multiple wavelengths yielded similar transition rates ranging form 8.4 to 19 s^{-1} depending on the studied arylguanidines (Table 1).

Whereas single turnover experiments in the presence of alkylguanidines, arylguanidines, and L-arginine exhibited a common kinetic trend, they revealed distinct kinetic parameters for Fe^{II}O$_2$ autoxidation (Table 1). L-Arginine- and agmatine-saturated iNOSoxy in the presence of BH$_2$ exhibited the same slow Fe^{II}O$_2$ decay. This decay was about 10 times faster when alkylguanidines **2** and **3** were present in the active site. In the case of arylguanidines **4**−**7**, it was up to 100 times faster than with L-arginine.

Influence of Alkyl- and Arylguanidines on Single-Turnover Reactions of BH$_4$-Containing iNOSoxy. Identical experiments have been conducted with BH$_4$-saturated iNOSoxy with substituted guanidines **1**−**7**. In the presence of L-arginine and any of the alkylguanidines **1**−**3**, iNOSoxy showed spectral changes that are similar to those previously observed with BH$_2$ (*14, 17*). The superimposed recorded spectra for alkylguanidines **2** and **3** are displayed in Figure 2A,B. Three different species were distinguished: an initial Fe^{II} at 412−415 nm, then a shoulder around 427 nm, and finally the Fe^{III} resting state at 395 nm. As observed with BH$_2$, buildup of Fe^{II}O$_2$ was too rapid to be accurately monitored, and its rate should be faster than 50 s^{-1}. In the presence of L-arginine, fitting of these characteristic wavelengths showed that Fe^{II}O$_2$ decay occurred at 20 s^{-1}. The global analysis of the superimposed spectra confirmed a two-steps kinetic model. The transition from ferrous iNOSoxy to the ferric form displayed only one transient species corresponding to Fe^{II}O$_2$ (peak at ∼427 nm) with a decay rate of 12 s^{-1}, as already

Table 1: Structures of the Studied Compounds and Kinetic Data Obtained for Single-Turnover Reactions of Ferrous iNOSoxy with O_2 in the Presence of BH_2 and Alkyl- or Arylguanidines **1**−**7**[a]

Compounds		Structures	k_1 $Fe^{II} \rightarrow Fe^{II}O_2 \rightarrow Fe^{III}$ k_1 (s^{-1})	k_2 k_2 (s^{-1})
L-arginine			> 50	0.2 ± 0.04
Agmatine	**1**		> 50	0.4 ± 0.14
$CF_3(CH_2)_3$guanidine	**2**		> 50	1.6 ± 0.5
Pentylguanidine	**3**		> 50	1.9 ± 0.4
2-Fphguanidine	**4**		> 50	8.4 ± 2.0
4-Fphguanidine	**5**		> 50	12.0 ± 3.0
4-Clphguanidine	**6**		> 50	7.3 ± 1.1
4-MeOphguanidine	**7**		> 50	18.9 ± 5.0

[a] Anaerobic solutions of ferrous iNOSoxy containing various substituted guanidines and BH_2 were rapidly mixed with air-saturated buffer at 10 °C to start the reaction, and heme transitions were followed by rapid-scanning UV−visible spectroscopy. The protein samples contained 250 μM BH_2, 10 mM L-arginine, or 30 mM of guanidines **1**−**7** in 50 mM HEPES buffer, pH 7.4, and were prepared as described in Materials and Methods. Data are means $\pm$ SD from three experiments.

reported (*41, 51*) (data not shown). The difference between the two rates calculated with the two distinct analytical procedures probably reflects the difficulty in extracting the spectrum of the first transient species.

The single-turnover experiments conducted with alkylguanidines **1**−**3** and BH_4 followed the same kinetic trend. The initial Fe^{II} species absorbing at 412−415 nm was converted into a species absorbing at 428−430 nm, depending on the bound alkylguanidines. This $Fe^{II}O_2$ intermediate further decayed to the Fe^{III} high-spin form of the heme absorbing at 393−395 nm. Figure 2E,F shows the spectra of $Fe^{II}O_2$ and Fe^{III} species for alkylguanidines **2** and **3** calculated with SPECFIT for a two-steps model, valid for all those alkylguanidines. Their buildup/decay kinetics are displayed in insets of Figure 2E,F, and the calculated kinetic

rates were around 1.5−2 times faster with compounds **1**−**3** than with L-arginine using either exponential fitting at specific wavelength or global analysis (Table 2).

Surprisingly, when iNOSoxy was saturated with arylguanidines **4**−**7**, the spectra only showed an initial species absorbing at 415 nm and the recovery of the ferric form at 395 nm. Figure 2C,D shows the spectra recorded with arylguanidines **4** and **6**. No transient species could be seen between this initial species and the final Fe^{III} state, and no shoulder at 427 nm was distinguishable from the visual inspection of spectra. The presence of clear isobestic points confirmed the absence of any observable intermediate and led us to fit these kinetics to monoexponential functions. The fittings of the absorbance cross sections at 395 and 650 nm (recovery of the high-spin Fe^{III} heme) gave apparent rate
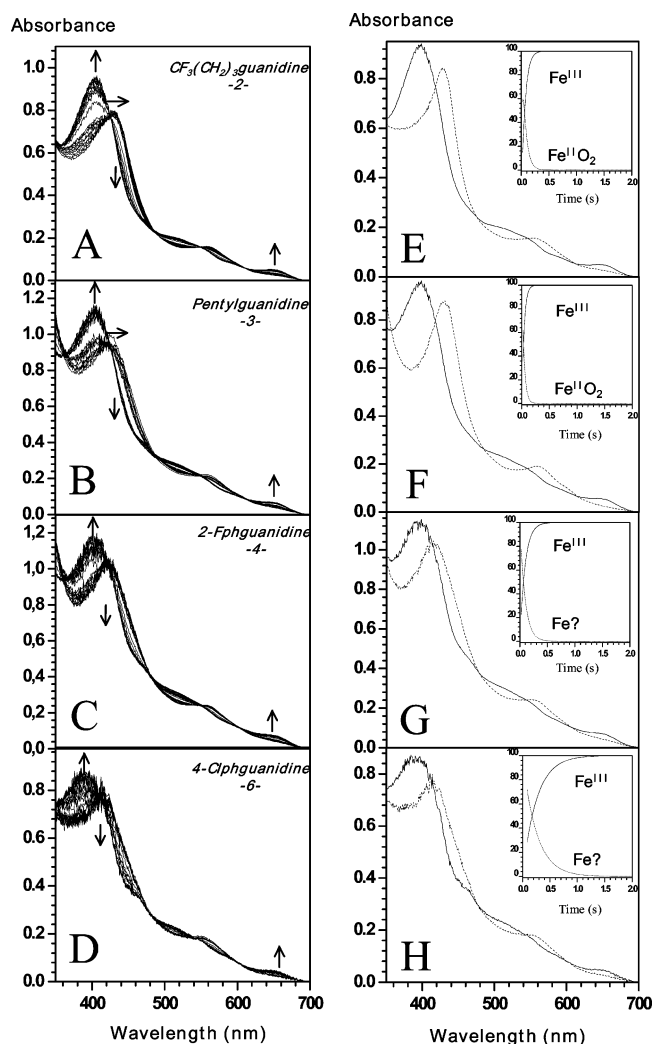
FIGURE 2: Heme transition in single-turnover reaction of BH_4-saturated iNOSoxy with O_2 in the presence of alkyl- and arylguanidines. Panels A−D show the superimposed spectra recorded after rapid-mixing at 10 °C of air-saturated buffer and dithionite-reduced iNOSoxy in the presence of BH_4 and $CF_3(CH_2)_3$-guanidine 2, pentylguanidine 3, 2-Fphguanidine 4, and 4-Clphguanidine 6, respectively. Panels E−F display the spectra of $Fe^{II}O_2$ and Fe^{III} in the presence of compounds 2, 3, 4, and 6 calculated by global analysis with SPECFIT/32. The insets display the resulting heme transition kinetics reported as percentage of the total heme transition.

Table 2: Kinetic Data Obtained for Single-Turnover Reactions of Ferrous iNOSoxy with O_2 in the Presence of BH_4 and Alkyl- or Arylguanidines 1−7[a]

| compounds | | $Fe^{II} \xrightarrow{k_1} Fe^{II}O_2 \xrightarrow{k_2} Fe^{III}$ | |
		k_1 (s^{-1})	k_2 (s^{-1})
L-arginine		>50	$20.5 \pm 2.0^b/12.7 \pm 0.6^c$
Agmatine	1	>50	$8.8 \pm 2.0^b/12.8 \pm 0.3^c$
$CF_3(CH_2)_3$guanidine	2	>50	$15.0 \pm 3.0^b/17.2 \pm 4.0^c$
Pentylguanidine	3	>50	$20.4 \pm 5.0^b/25.5 \pm 3.0^c$

| compounds | | $Fe^{II} -(- - -) \xrightarrow{k} Fe^{III}$ |
		k (s^{-1})
2-Fphguanidine	4	$20.5 \pm 1.5^b/12.6 \pm 0.3^c$
4-Fphguanidine	5	$9.0 \pm 0.7^b/4.3 \pm 0.2^c$
4-Clphguanidine	6	$12.3 \pm 1.8^b/4.5 \pm 0.3^c$
4-MeOphguanidine	7	$31.0 \pm 2.0^b/9.3 \pm 0.9^c$

[a] Anaerobic solutions of ferrous iNOSoxy containing substituted guanidines 1−7 and BH_4 were rapidly mixed with air-saturated buffer at 10 °C to start the reaction, and heme transitions were followed by rapid-scanning UV−visible spectroscopy. The protein samples containing 100 μM BH_4 were prepared in the presence of 10 mM L-arginine or 30 mM of guanidines 1−7 in 50 mM HEPES buffer, pH 7.4, as described in Materials and Methods. Data are means $\pm$ SD from three experiments. [b] Rates determined by monoexponential fitting at single wavelengths (427, 650, and 395 nm). [c] Rates determined by SPECFIT global analysis.

$Fe^{II}O_2$ complex. Alkylguanidines 2 and 3 induced a decay of $Fe^{II}O_2$ 10-fold faster than L-arginine did. This destabilization was dramatically enhanced in the presence of arylguanidines 4−7 and was 100 times faster than with L-arginine. Finally, experiments performed with BH_4-saturated iNOSoxy showed different oxygen activation processes between alkylguanidines and arylguanidines as no $Fe^{II}O_2$ intermediate could be observed with arylguanidines 4−7.

To better understand how alkyl- and arylguanidines could differently influence $Fe^{II}O_2$ stabilization and oxygen activation, we used the $Fe^{II}CO$ complex as a stable surrogate for the $Fe^{II}O_2$ intermediate and studied the influence of alkylguanidines 2 and 3 and arylguanidines 5 and 6 on the vibration frequencies of iNOSoxy $Fe^{II}CO$ saturated with BH_4 by RR and FTIR spectroscopy.

Resonance Raman Spectra of iNOSoxy $Fe^{II}CO$ in the Presence of Alkyl- and Arylguanidines. Resonance Raman spectra of the iNOSoxy $Fe^{II}CO$ complex in the presence of BH_4 and guanidines 2, 3, 5, and 6 were obtained with a 441.6 nm laser excitation. The high-frequency region of the spectra exhibited markers ν_4, ν_3, and ν_2, specific to the oxidation, spin, and coordination states of the heme iron (11, 43, 45, 46, 52). The ν_4, ν_3, and ν_2 frequencies were found at 1367, 1463, and 1569 cm^{-1}, respectively, in the presence of all the alkyl- and arylguanidines tested and corresponded to values previously observed for NOS $Fe^{II}CO$ complexes (43, 45, 46) (data not shown). These porphyrin modes thus remained unaltered in the presence of all the tested compounds that did not seem to alter the structure of the heme. This was confirmed in the low-frequency regions by the values of ν_{16}, ν_7, and ν_8 frequencies that were, respectively, observed at 750, 678, and 340 cm^{-1} and corresponded to low-spin hexacoordinated $Fe^{II}CO$ species (11, 52). A RR spectrum of Fe^{II} iNOSoxy has been recorded under the same conditions and enabled us to assign the minor bands at ∼692, 1345, 1388, 1420, and 1600 cm^{-1} as resulting from the partial

constants ranging from 9 to 31 s^{-1} for all compounds (Table 2). Single-value decomposition analysis, when forced to proceed in two or three steps, also failed to show any transient species between the initial and final species. Therefore, we chose to fit the data to a simple "A → B" model. Figure 2G,H shows the two calculated spectra obtained when arylguanidines 4 and 6 were bound. The first spectra with a Soret peak at 414−416 nm converted to the ferric form (∼395 nm) with transition rates varying between 4 and 31 s^{-1} depending on the arylguanidines and the analytical method used for calculation (Table 2 and insets of Figure 2G,H, for 4 and 6).

From these two sets of single turnover experiments, three major conclusions can be drawn. First, single-turnover reactions with BH_2 showed that all bound alkyl- or arylguanidines studied did not seem to modify the kinetics of oxygen binding to the ferrous heme. Second, binding of non-amino acid guanidine derivatives greatly destabilized the
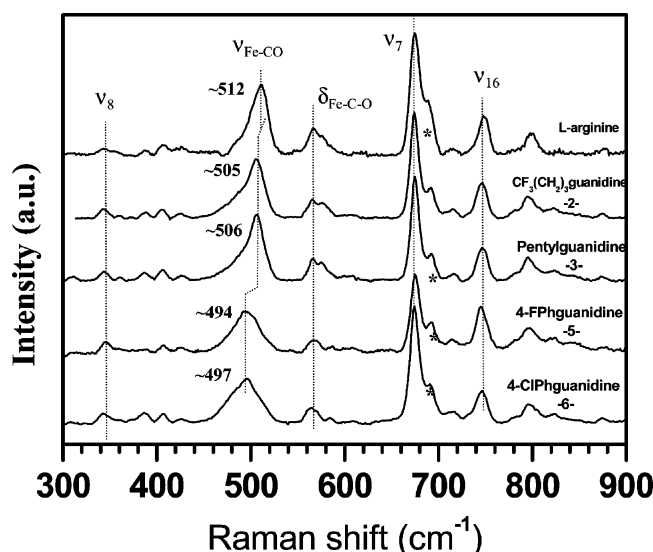
FIGURE 3: Resonance Raman spectra in the low-frequency region of iNOSoxy ferrous heme—CO complexes in the presence of alkyl- and arylguanidines. The spectra were recorded at room temperature in 0.1 M potassium phosphate buffer containing 150—200 μM iNOSoxy Fe^{II}CO in the presence of 10 mM of substituted guanidines **2**, **3**, **5**, or **6**, 3 mM DTT, and 400 μM BH$_4$ as described under Materials and Methods. The lines marked by * correspond to the contribution from ferrous species due to partial CO photodissociation. The laser excitation wavelength was 441.6 nm. All spectra are baseline-corrected.

photodissociation of CO from the ferrous heme (data not shown) (*43, 44, 53*).

Low-frequency regions of the resonance Raman spectra showed clear differences as a function of the compound bound at the active site (Figure 3). By the usage of isotope labeling, several studies have assigned the stretching (ν_{Fe-CO}) and bending (δ_{Fe-CO}) modes frequencies of iNOSoxy Fe^{II}-CO moiety at 490—512 and ~560 cm^{-1}, respectively (*45*). In the absence of substrate and cofactors, NOS ν_{Fe-CO} RR modes appear as broad bands (ca. 35—40 cm^{-1} fwhm) (*43, 45*) due to the contributions from different ν_{Fe-CO} bands corresponding to different heme distal pocket protein interactions with the CO ligand that affect both the ν_{Fe-CO} and ν_{C-O} frequencies. The Fe^{II}CO substrate-free iNOS complexes have been described in two different conformations: an "open" conformation characterized by low ν_{Fe-CO} (around 479 cm^{-1}) and high ν_{CO} (around 1945 cm^{-1}) frequencies and a "closed" conformation with higher ν_{Fe-CO} (around 499 cm^{-1}) and lower ν_{CO} (around 1930 cm^{-1} in iNOS) frequencies (*43, 46, 54*). In the absence of L-arginine and BH$_4$, we observed a broad ν_{Fe-CO} RR band (ca. 35—40 cm^{-1} fwhm) at 491 cm^{-1} and a ν_{C-O} FTIR band at 1943 cm^{-1} (30 cm^{-1} fwhm) (data not shown). L-Arginine binding has been shown to induce the disappearance of the open conformation and a strengthening of the iNOS Fe—CO bond (ν_{Fe-CO} and ν_{CO} at 512 and 1905 cm^{-1}, respectively) (*43, 54*). Indeed, upon L-arginine and H$_4$B binding, the iNOSoxy ν_{CO} FTIR band narrowed (12 cm^{-1} fwhm) and shifted to 1902 cm^{-1}, reflecting a more homogeneous distal pocket environment. This was confirmed by RR experiments that showed a narrower ν_{Fe-CO} RR band at 512 cm^{-1} (Figures 3 and 4).

These former analyses enabled us to identify the frequencies corresponding to ν_{Fe-CO} and δ_{Fe-CO} modes in our RR experiments (Figure 3, Table 3). On one hand, the alky-
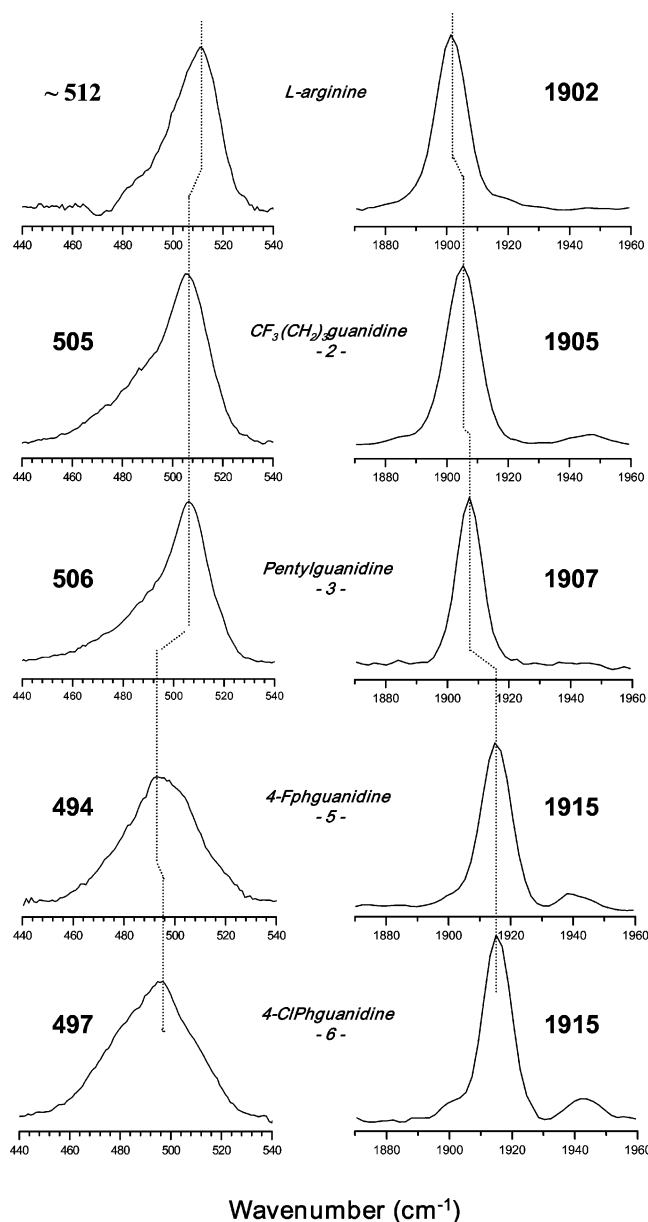

FIGURE 4: Resonance Raman and FTIR spectra showing the Fe—CO and CO vibration modes for iNOSoxy in the presence of guanidine derivatives. Left column, part of the RR spectra showing the ν_{Fe-CO} bands recorded for BH$_4$-saturated iNOSoxy Fe^{II}CO complexes in the presence of alkylguanidines **2** and **3** and arylguanidines **5** and **6**. Right column, part of the corresponding FTIR spectra showing the ν_{CO} vibration mode.

lguanidines induced a shift of the Fe—CO stretch RR band maximum from 491 cm^{-1} (substrate-free iNOS) to 505 cm^{-1}, reminiscent of the disappearance of the open conformation observed upon L-arginine binding (*45, 46*). On the other hand, upon binding of the arylguanidines, the Fe—CO stretching frequency remained consistently around 494—497 cm^{-1}. This smaller shift could reflect a slight reduction of the proportion of the open form and/or an increase of the ν_{Fe-CO} frequency of the closed form. The bending modes of Fe—CO were also found different for alkyl- and arylguanidines. In the presence of arylguanidines, the Fe^{II}CO complex displayed a weak band at 563—565 cm^{-1}, similar to what has been reported for the substrate-free enzyme (*46*). The addition of alkylguanidines induced a shift of the δ_{Fe-CO} frequency that was also observed upon L-arginine binding (*46*).

Table 3: Frequencies of the ν_{Fe-CO}, δ_{Fe-CO}, and ν_{CO} Lines of the $Fe^{II}CO$ Complexes of iNOSoxy in the Presence of BH_4 and Substituted Guanidines **2**, **3**, **5**, and **6** Measured by RR and FTIR[a]

	compounds		ν_{Fe-CO} (cm^{-1})	δ_{Fe-CO} (cm^{-1})	ν_{CO} (cm^{-1})
	without substrate		491	562	1946
	L-arginine		512[b,c]	569[b,c]	1905[b]/1902[c]
Alkylguanidines	CF$_3$(CH$_2$)$_3$guanidine	**2**	505	566	1905
	pentylguanidine	**3**	506	567	1907
Arylguanidines	4-Fphguanidine	**5**	494	563	1915
	4-Clphguanidine	**6**	497	565	1915

[a] The protein samples contained 30 mM of the studied compounds and 100 μM BH$_4$ and were prepared as described under Materials and Methods. RR and FTIR spectra were recorded at room temperature, and analyses of data were performed as described under Materials and Methods. [b] Values taken from refs *45, 46, 54*. [c] This work.

Thus, arylguanidines seemed to have a small effect on the Fe−CO vibration frequencies, whereas alkylguanidines seemed to significantly modify the environment of the bound CO.

Effect of Alkyl- and Arylguanidines on the CO Vibration Mode Studied by ATR-FTIR. Figure 4, right panels, displays the iNOSoxy Fe^{II}CO FTIR spectra recorded in the presence of the alkyl- (**2**, **3**) and arylguanidines (**5**, **6**). For each substituted guanidine, the FTIR spectra exhibit one major band contribution between 1905 and 1915 cm^{-1}, all with narrow bandwidths (ca. 13 cm^{-1}). In the case of alkylguanidines **2** and **3**, the ν_{CO} frequency was observed at about 1905 cm^{-1}. This very narrow band at 1905 cm^{-1} was similar to the value previously reported for iNOS with bound L-arginine (*54*) (Table 3), indicating an homogeneous closed conformation. In the presence of arylguanidines **4** and **5**, the ν_{CO} band was seen at a higher frequency (1915 cm^{-1}). This significant shift from 1940 to 1915 cm^{-1} argued for a closed conformation, but one that is slightly different from that observed in the presence of L-arginine and the alkylguanidines.

For some compounds, and more significantly for arylguanidines **5** and **6**, a very weak band between 1940 and 1950 cm^{-1} was observed that could be due to minor populations of the remaining open conformation.

Resonance Raman and ATR−FTIR data both underline the distinct effects of alkyl- and arylguanidines on the iNOS heme pocket conformations: while alkylguanidines **2** and **3**, similar to L-arginine, are able to significantly alter CO coordination, arylguanidines **5** and **6** only slightly modify the open/closed ratio and/or the Fe−CO bond strength.

DISCUSSION

Inducible NOS is able to produce NO from oxidation of some alkylguanidines, whereas in the presence of arylguanidines, NADPH oxidation exclusively results in the release of superoxide ion and hydrogen peroxide (*30, 33*). This uncoupling can arise from two pathways: either the intermediate Fe^{II}O$_2$ complex can decompose into Fe^{III} and O$_2^{\bullet-}$, or hydrogen peroxide can be formed during the oxygen activation mechanism after protonation of ferric hydroperoxo complex (Fe^{III}OOH) (*10, 34, 35, 55, 56*). To understand how alkyl- and arylguanidines can influence these pathways, we first investigated the kinetics of Fe^{II}O$_2$ autoxidation and

activation. Modification of the heme Fe^{II}O$_2$ structure in the presence of alkyl- and arylguanidines was examined using RR and FTIR spectroscopies with the more stable iNOS Fe^{II}-CO complex as a probe.

Stability of Fe^{II}O$_2$ Complex in the Presence of Alkyl- and Arylguanidines. Rapid-mixing stopped-flow experiments have been conducted with iNOSoxy containing BH$_2$, a BH$_4$ analogue that does not transfer electrons to the Fe^{II}O$_2$ intermediate (*37, 57*). In these conditions, we were able to characterize the stability of iNOSoxy Fe^{II}O$_2$ as a function of the nature of the substituted guanidines. For all sets of experiments, heme transitions followed the kinetic scheme observed with L-arginine (*41*): initial Fe^{II} state, followed by the binding of dioxygen leading to Fe^{II}O$_2$, and finally the recovery of the resting Fe^{III} state. Oxygen binding on Fe^{II} species occurred too fast to be accurately monitored by our detector, and its rates were thus estimated to be greater than 50 s^{-1} without significant effect of alkylguanidines and arylguanidines bound in the active site. Rates of the subsequent Fe^{II}O$_2$ decay followed the following order: arylguanidines (100 times faster than with L-arginine) > alkylguanidines (10 times faster) > L-arginine, agmatine. This suggests that the presence of alkyl- or arylguanidines could not stabilize the Fe^{II}O$_2$ species to the same extent as L-arginine did. This could arise either from a binding of these guanidines further above the heme or from a weaker polar interaction between the heme dioxygen complex and the substituted guanidines. To obtain more information on the structural features that could account for this Fe^{II}O$_2$ instability, we used the more stable Fe^{II}CO complex as a surrogate and studied iNOSoxy Fe^{II}CO complexes in the presence of these different compounds by RR and ATR−FTIR. Although Fe^{II}CO, Fe^{II}NO, and Fe^{II}O$_2$ complexes display different geometry, diatomic ligands CO and NO have been used to investigate the interactions of L-arginine analogues with the active site of NOS (*11, 47, 58−60*). In fact, Fe^{II}CO complexes are much more stable than Fe^{II}NO and Fe^{II}O$_2$ ones and are thus very useful probes for the active site of heme proteins (*47, 58, 59*).

Fe^{II}CO Vibration Modes in the Presence of Alkyl- and Arylguanidines. The analysis of the Fe−CO stretching mode (ν_{Fe-CO}) in the RR spectra of Fe^{II}CO complexes is somewhat complicated due to the presence of minor contributions of ferrous heme and of Fe^{II}CO porphyrin vibration modes (*43, 45, 54*). All RR spectra displayed a small ferrous heme contribution due to partial photodissociation of the CO from the heme induced by alkyl- and arylguanidines. This artifactual phenomenon has already been observed in iNOS and nNOS as well as with P450$_{scc}$ and P450$_{cam}$ where binding of a substrate or analogue in the distal heme pocket region enhanced CO photodissociation (*43, 44, 53*). Fitting analysis of the complex ν_{Fe-CO} band showed contribution of a component at 512 cm^{-1} linked to the enhancement of a porphyrin mode arising from Fermi resonance coupling due to its near-degeneracy with ν_{Fe-CO} frequency (*43, 61*) (data not shown).

Despite the identification of ferrous and Fe^{II}CO porphyrin modes contributions, RR spectra assignment remained complicated by uncertainties on the number and nature of Fe^{II}-CO conformations. Indeed, Fe^{II}CO substrate-free NOS complexes exist in two different conformations, "open" and "closed". Furthermore, L-arginine binding to iNOS induces

the suppression of the open form (*43*) and a shift of the ν_{Fe-CO} frequency (11−12 cm^{-1}) (*43*, *45*, *46*). Thus, we used the simpler FTIR data in the ν_{CO} region to determine the number and nature of Fe^{II}CO conformations and only considered the observed apparent maximum of the complex broad ν_{Fe-CO} RR band. Both analyses were interconnected using the inverse relationship between ν_{Fe-CO} and ν_{CO} modes (*58*).

We observed different shifts upon substituted guanidine binding which implies that the guanidinium/CO interaction is slightly different with respect to substrate bound in the heme pocket. FTIR data show a dominant narrow (ca. 12 cm^{-1} fwhm) band with a low ν_{CO} frequency at 1905−1907 cm^{-1} with alkylguanidines **2** and **3** (this report) or at 1902−1905 cm^{-1} with L-arginine (this report, *45*, *46*). Similar to L-arginine, binding of **2** and **3** leads to a homogeneous closed conformation where the CO ligand is significantly interacting with the positively charged guanidium group, and is most likely engaged in H-bonding (*54*). However, the interaction is not strictly identical as compared to L-arginine. Whereas L-arginine-bound iNOS exhibits a ν_{Fe-CO} RR band at 512 cm^{-1}, the alklyguanidine binding results in a RR band at 505 cm^{-1}. The observation that the ν_{Fe-CO} frequencies are different while the ν_{CO} frequencies remain largely unchanged is a strong indication that the positive polarity around the oxygen atom is similar but the Fe−CO tilt angle could be larger for the alkylguanidines (lower ν_{Fe-CO}) than for the L-arginine (higher ν_{Fe-CO}) (*58*).

For the arylguanidines **5** and **6**, FTIR data show a major narrow CO band at 1915 cm^{-1}. The narrow bandwidth again indicates a very homogeneous major closed population. Although the ν_{CO} frequency is relatively higher than those of alkylguanidines (+10 cm^{-1}) it cannot be associated to an open conformation for which ν_{CO} frequency ranges between 1930 and 1950 cm^{-1} (*54*). The relatively high frequency of 1915 cm^{-1} in the FTIR spectra correlates well with the relatively lower ν_{Fe-CO} frequency seen in the RR spectra (Figure 4) and indicates a less positive polarity around the CO environment as compared to the alkylguanidines and the L-arginine.

Origin of the Observed Differences of Fe^{II}CO Vibration Modes. It has been shown for the cytochrome P450 enzymes and other heme proteins that electrostatic effects more than steric constraints may have a major effect on ν_{CO} and ν_{Fe-CO} frequencies (*58*, *59*, *62*, *63*). Introducing a positive charge (L-arginine guanidinium) toward the heme Fe^{II}CO complex would stabilize the negative charge borne by the oxygen of CO leading to the mesomeric form Fe$^{\delta+}$=C=O$^{\delta-}$ and thus lowering the bond order of CO and increasing that of Fe−C (*58*, *59*). Thus, the differences of ν_{FeCO} and ν_{CO} frequencies observed between all substituted guanidines and L-arginine seem to be due to a different polar environment in the Fe^{II}-CO vicinity. This could arise from a greater distance between the bound guanidines and the CO ligand, which would alleviate the positive charge and also weaken the purported H-bond. However, as indicated by Fan et al., if the difference in ν_{Fe-CO} frequency was related to the binding of compounds further from the heme, the 5−7 cm^{-1} shift we observed would correspond to almost 1 Å difference in distance (*45*). This could be too large considering the fact that the alkylguanidines **2** and **3** remain transformed into NO• (*33*). Thus, changes in ν_{Fe-CO} and ν_{CO} frequencies are likely to arise from a different polar environment in Fe^{II}CO vicinity.
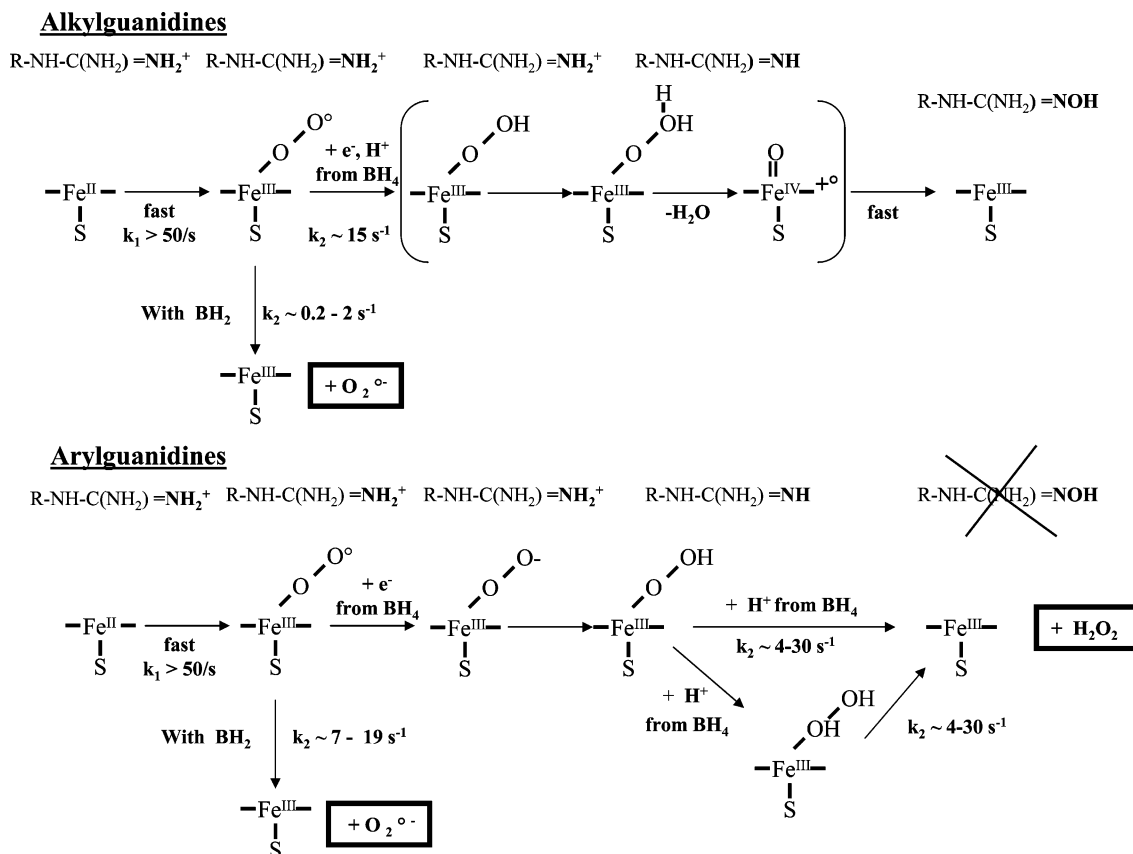
With alkylguanidines, the positive guanidinium moiety remains able to exert the same effect on Fe^{II}CO but to a lesser extent compared to L-arginine. There is no X-ray structure of iNOS crystallized with these guanidine derivatives to assess their positioning in the active site. However, the structures of some non-amino acid hydroxyguanidines crystallized in n- and eNOS active sites show that the hydroxyguanidinium moiety always establishes electrostatic interactions with Glu592 and Glu363, respectively, but the butyl- or chlorophenyl-substituents of these guanidines are directed toward a hydrophobic pocket comprising Val, Pro, and Phe residues (*64*, *65*). The guanidinium moiety of alkyl- or arylguanidines should remain close to the heme, but these distinct binding conformations may not exert as strong interactions with the heme−CO complex as with L-arginine. Subtle changes in alkylguanidines binding in the heme pocket could explain variations in the Fe−CO tilt geometry and in the interaction between alkylguanidines and the bound CO.

In the case of arylguanidines, our vibrational data indicate a significant decrease of the positive polarity around the CO environment as compared to L-arginine or alkylguanidines binding. The possibility that the arylguanidines could fail in establishing the expected H-bond between the L-arginine guanidinium and the Fe−CO complex (*46*, *54*) is not consistent with our FTIR results which clearly show a strong polar interaction between CO and the distal heme pocket. Thus, this H-bond is likely to exist with arylguanidines, despite the small shifts of ν_{Fe-CO} frequencies. Another interpretation is that, with these compounds, the presence of a phenyl ring conjugated with the positive guanidinium allows the positive charge to be fully delocalized on the molecule. The effective charge borne by the guanidinium moiety of the arylguanidines, purportedly near the CO ligand, should be smaller. This will lower the positive charge around CO and may not favor as much the Fe$^{\delta+}$=C=O$^{\delta-}$ form in the mesomeric equilibrium (*62*, *63*).

Both FTIR and RR data suggest that, like L-arginine, alkylguanidines are able to strongly modify CO coordination to ferrous heme, whereas a significantly lower positive polarity is observed around the complex in the presence of arylguanidines.

Implications of the Modification of Polar Environment in the Active Site. We observed a good correlation between heme pocket polarity, Fe^{II}O$_2$ stability, electron coupling, and NO formation that followed the order: L-arginine > alkylguanidines > arylguanidines (*6*, *33*).

The stabilization of the Fe$^{\delta+}$=C=O$^{\delta-}$ form of Fe^{II}CO by L-arginine (polar effect signaled above) could reflect that L-arginine stabilizes Fe^{II}O$_2$ and prevents its dissociation into Fe^{III} and O$_2$•$^-$. Since Fe^{II}O$_2$ autoxidation is in competition with oxygen activation, increases in autoxidation rates will lead to electron uncoupling. Alkylguanidines induced less polar interactions with Fe^{II}CO and could not be able to favor the negative charge on the distal oxygen and stabilize Fe^{II}O$_2$ complexes as well as L-arginine. As a consequence, decay of Fe^{II}O$_2$ is accelerated by 10 times, but, even if superoxide is generated, alkylguanidines are still precursors of NO. With arylguanidines, the interaction may be so dramatically decreased that Fe^{II}O$_2$ becomes very unstable and decays with rates that can be up to 100 times that observed for L-arginine. Rates of Fe^{II}O$_2$ autoxidation then might be so fast that iNOS generates superoxyde instead of NO.

Scheme 1: Proposed Mechanisms for the First Step of Oxygen Activation by INOSoxy in the Presence of Alkyl- and Arylguanidines[a]

Alkylguanidines

$R\text{-}NH\text{-}C(NH_2)=NH_2^+$ $R\text{-}NH\text{-}C(NH_2)=NH_2^+$ $R\text{-}NH\text{-}C(NH_2)=NH_2^+$ $R\text{-}NH\text{-}C(NH_2)=NH$ $R\text{-}NH\text{-}C(NH_2)=NOH$

$-Fe^{II}-$ $\xrightarrow[k_1 > 50/s]{fast}$ $-Fe^{III}-$ $\xrightarrow[k_2 \sim 15\ s^{-1}]{+\ e^-,\ H^+\ from\ BH_4}$ $\left[\ -Fe^{III}- \rightarrow -Fe^{III}- \xrightarrow{-H_2O} -Fe^{IV}-{}^{+\circ}\ \right]$ $\xrightarrow{fast}$ $-Fe^{III}-$

With BH_2 $k_2 \sim 0.2 - 2\ s^{-1}$

$-Fe^{III}-$ $+\ O_2{}^{\circ-}$

Arylguanidines

$R\text{-}NH\text{-}C(NH_2)=NH_2^+$ $R\text{-}NH\text{-}C(NH_2)=NH_2^+$ $R\text{-}NH\text{-}C(NH_2)=NH_2^+$ $R\text{-}NH\text{-}C(NH_2)=NH$ ~~$R\text{-}NH\text{-}C(NH_2)=NOH$~~

$-Fe^{II}-$ $\xrightarrow[k_1 > 50/s]{fast}$ $-Fe^{III}-$ $\xrightarrow{+\ e^-\ from\ BH_4}$ $-Fe^{III}-$ $\rightarrow$ $-Fe^{III}-$ $\xrightarrow[k_2 \sim 4\text{-}30\ s^{-1}]{+\ H^+\ from\ BH_4}$ $-Fe^{III}-$ $+\ H_2O_2$

With BH_2 $k_2 \sim 7 - 19\ s^{-1}$

$+\ H^+$ from BH_4 $k_2 \sim 4\text{-}30\ s^{-1}$ $-Fe^{III}-$

$-Fe^{III}-$ $+\ O_2{}^{\circ -}$

[a] Top panel, proposed mechanism pathway with either BH_2 or BH_4 in the presence of L-arginine or alkylguanidines. Bottom panel, proposed mechanism with BH_2 or BH_4 in the presence of arylguanidines.

Influence of Alkylguanidines on Oxygen Activation Steps. In the generally accepted mechanism of L-arginine oxidation, one electron and one proton from BH_4 are rapidly transferred to $Fe^{II}O_2$ and lead to $Fe^{III}OOH$ (*19−21, 42*). Then, a second proton, presumably from L-arginine guanidinium (*66*), is transferred to $Fe^{III}OOH$. When electron and proton transfers are synchronous, the first protonation is favored on the distal oxygen followed by a second protonation of the same oxygen leading to $Fe^{III}(OOHH)$ that rapidly converts into the hydroxylating agent $Fe^{IV}(=O)$ and H_2O (Scheme 1). With L-arginine, the electron-transfer rate is high enough to overcome $Fe^{II}O_2$ autoxidation (100 times faster). This leads to a significant buildup of $Fe^{IV}(=O)$ and consequent NO formation without electron uncoupling.

In the presence of alkylguanidines, the transitions follow the same kinetic scheme: BH_4 donates one electron and one proton to $Fe^{II}O_2$ species that promotes the rapid formation of the hydroxylating agent $Fe^{IV}(=O)$ (Scheme 1). The activation of $Fe^{II}O_2$ ($\sim 20\ s^{-1}$, Table 2) is only 10 times faster than $Fe^{II}O_2$ autoxidation (1.6−1.9 s^{-1}, Table 1). Thus, competition between these two pathways results in electron uncoupling and formation of $O_2{}^{\bullet-}$ ($Fe^{II}O_2$ autoxidation to Fe^{III} and $O_2{}^{\bullet-}$). This can explain the uncoupling and the less efficient formation of NO reported for alkylguanidines **2** and **3** (*33*).

A Different Mechanism Pathway in the Presence of Arylguanidines. In the presence of arylguanidines **4−7** and BH_4, single-turnover experiments failed to show any $Fe^{II}O_2$ intermediate species absorbing around 430 nm: the initial species (413−416 nm) directly decays into Fe^{III} resting state with no transient accumulation of the $Fe^{II}O_2$ complex (Figure 2C,D). Because the iNOSoxy $Fe^{II}O_2$ spectra were detectable in the presence of BH_2, O_2 binding kinetics should not be modified in the presence of arylguanidines. Moreover, in these experiments with BH_2, this $Fe^{II}O_2$ intermediate absorbed at 428−430 nm and corresponded to an $Fe^{II}O_2$ "heme−oxy II complex" (*42*). We then ruled out the possibility that the species absorbing around 415 nm in BH_4-saturated iNOSoxy experiments could correspond to the "heme−oxy I complex" absorbing at 418 nm (*42*). Last, with nNOSoxy and eNOSoxy, no $Fe^{II}O_2$ was observed in the absence of substrate while conducting single-turnover experiments (*21, 22*). However, we excluded the absence of substrate binding at the active site because (i) we were at concentrations exceeding 50 times the dissociation constants of the arylguanidines (*67*), (ii) the FTIR spectra confirmed the binding of all arylguanidines to iNOSoxy, and (iii) our decay rates did not match those reported by Ost et al. and Berka et al. for nNOSoxy and eNOSoxy (*21, 22*).

We suggest that the unusual catalytic behavior of BH_4-saturated iNOSoxy in the presence of our arylguanidines was linked to the properties of the arylguanidines themselves. This could be related to differences in the polarity of the heme pocket but could also arise from differences in pK_a. Due to the existence of resonance forms for arylguanidines, their guanidinium group has a lower pK_a than the alkylguanidines and L-arginine one ($pK_a \sim 11$ and ~ 13, respectively) (*68*). With arylguanidines, we propose that the first

proton would be supplied by the arylguanidine that offers a very labile proton. This would result in asynchronous electron−proton transfers from BH$_4$ (see Scheme 1). Theoretical calculations on P450 models suggest that, for asynchronous electron and proton transfers, the second proton would preferably bind to the proximal oxygen leading to Fe^{III}-(HOOH) that will further decompose into H$_2$O$_2$ and Fe^{III} (69). This nonproductive cycle would explain the high electron uncoupling observed with the arylguanidines and could contribute to the high amounts of H$_2$O$_2$ produced (unpublished data).

Nonetheless, the rate-limiting step observed in the presence of arylguanidines remains undetermined. Since no spectrum for Fe^{II}O$_2$ complex was observed, Fe^{II}O$_2$ activation should occur very rapidly, probably due to changes in the electric field induced by arylguanidines and/or a more acidic proton of the guanidinium group of arylguanidines. The slow rate-limiting step in the presence of arylguanidies (Table 2) must take place later in the catalytic chain and could then correspond to the decay of either Fe^{III}OOH or Fe^{III}HOOH species (Scheme 1).

Our single-turnover stopped-flow experiments combined with our spectroscopic studies showed that substrates could up- or down-regulate electron uncoupling and reactive oxygen species production, that is, H$_2$O$_2$ and O$_2$$^{•-}$ by iNOS. Using arylguanidines as a tool to investigate iNOS oxidation mechanism, we suggest that electron and proton transfers in iNOS must occur synchronously to prevent electron uncoupling and oxidase activity of iNOS.

ACKNOWLEDGMENT

REFERENCES

1. Ignarro, L. J. (2000) *Nitric Oxide: Biology and Pathobiology* (Ignarro, L. J., Ed.) Academic Press, San Diego, CA.

2. Alderton, W. K., Cooper, C. E., and Knowles, R. G. (2001) Nitric oxide synthases: structure, function and inhibition, *Biochem. J. 357*, 593−615.

3. Pfeiffer, S., Mayer, B., and Hemmens, B. (1999) Nitric oxide: chemical puzzles posed by a biological messenger, *Angew. Chem., Int. Ed. 38*, 1715−1731.

4. Vallance, P. (2003) Nitric oxide: therapeutic opportunities, *Fundam. Clin. Pharmacol. 17*, 1−10.

5. Babu, B. R., and Griffith, O. W. (1998) Design of isoform-selective inhibitors of nitric oxide synthase, *Curr. Opin. Chem. Biol. 2*, 491−500.

6. Mansuy, D., and Boucher, J.-L. (2004) Alternative nitric oxide-producing substrates for no synthases, *Free Radical Biol. Med. 37*, 1105−1121.

7. Groves, J. T., and Wang, C. C.-Y. (2000) Nitric oxide synthase: models and mechanisms, *Curr. Opin. Chem. Biol. 4*, 687−695.

8. Werner, E. R., Gorren, A. C., Heller, R., Werner-Felmayer, G., and Mayer, B. (2003) Tetrahydrobiopterin and nitric oxide: mechanistic and pharmacological aspects, *Exp. Biol. Med. (Maywood, NJ) 228*, 1291−1302.

9. Stuehr, D. J., Santolini, J., Wang, Z. Q., Wei, C. C., and Adak, S. (2004) Update on mechanism and catalytic regulation in the NO synthases, *J. Biol. Chem. 279*, 36167−36170.

10. Li, H., and Poulos, T. L. (2005) Structure−function studies on nitric oxide synthases, *J. Inorg. Biochem. 99*, 293−305.

11. Rousseau, D. L., Li, D., Couture, M., and Yeh, S. R. (2005) Ligand-protein interactions in nitric oxide synthase, *J. Inorg. Biochem. 99*, 306−323.

12. Bredt, D. S., Hwang, P. M., Glatt, C. E., Lowenstein, C., Reed, R. R., and Snyder, S. H. (1991) Cloned and expressed nitric oxide synthase structurally resembles cytochrome P450 reductase, *Nature 351*, 714−718.

13. Masters, B. S. S., McMillan, K., Sheta, E. A., Nishimura, J. S., Roman, L. J., and Martasek, P. (1996) Neuronal nitric oxide synthase, a modular enzyme formed by convergent evolution: structure studies of a cysteine thiolate-liganded heme protein that hydroxylates L-arginine to produce NO as a cellular signal, *FASEB J. 10*, 552−558.

14. Boggs, S., Huang, L., and Stuehr, D. J. (2000) Formation and reactions of the heme-dioxygen intermediate in the first and second steps of nitric oxide synthesis as studied by stopped-flow spectroscopy under single-turnover conditions, *Biochemistry 39*, 2332−2339.

15. Bec, N., Gorren, A. C., Voelker, C., Mayer, B., and Lange, R. (1998) Reaction of neuronal nitric-oxide synthase with oxygen at low temperature. Evidence for reductive activation of the oxy-ferrous complex by tetrahydrobiopterin, *J. Biol. Chem. 273*, 13502−13508.

16. Hurshman, A. R., Krebs, C., Edmondson, D. E., Huynh, B. H., and Marletta, M. A. (1999) Formation of a pterin radical in the reaction of the heme domain of inducible nitric oxide synthase with oxygen, *Biochemistry 38*, 15689−15696.

17. Wei, C. C., Wang, Z. Q., Wang, Q., Meade, A. L., Hemann, C., Hille, R., and Stuehr, D. J. (2001) Rapid kinetic studies link tetrahydrobiopterin radical formation to heme-dioxy reduction and arginine hydroxylation in inducible nitric-oxide synthase, *J. Biol. Chem. 276*, 315−319.

18. Davydov, R., Ledbetter-Rogers, A., Martasek, P., Larukhin, M., Sono, M., Dawson, J. H., Masters, B. S. S., and Hoffman, B. M. (2002) EPR and ENDOR characterization of intermediates in the cryoreduced oxy-nitric oxide synthase heme domain with bound L-arginine or N^G-hydroxyarginine, *Biochemistry 41*, 10375−10381.

19. Wei, C. C., Wang, Z. Q., Arvai, A. S., Hemann, C., Hille, R., Getzoff, E. D., and Stuehr, D. J. (2003) Structure of tetrahydrobiopterin tunes its electron transfer to the heme−dioxy intermediate in nitric oxide synthase, *Biochemistry 42*, 1969−1977.

20. Sorlie, M., Gorren, A. C., Marchal, S., Shimizu, T., Lange, R., Andersson, K. K., and Mayer, B. (2003) Single-turnover of nitric-oxide synthase in the presence of 4-amino-tetrahydrobiopterin: proposed role for tetrahydrobiopterin as a proton donor, *J. Biol. Chem. 278*, 48602−48610.

21. Berka, V., Yeh, H. C., Gao, D., Kiran, F., and Tsai, A. L. (2004) Redox function of tetrahydrobiopterin and effect of L-arginine on oxygen binding in endothelial nitric oxide synthase, *Biochemistry 43*, 13137−13148.

22. Ost, T. W., and Daff, S. (2005) Thermodynamic and kinetic analysis of the nitrosyl, carbonyl, and dioxy heme complexes of neuronal nitric-oxide synthase. The roles of substrate and tetrahydrobiopterin in oxygen activation, *J. Biol. Chem. 280*, 965−973.

23. Meunier, B., de Visser, S. P., and Shaik, S. (2004) Mechanism of oxidation reactions catalyzed by cytochrome P450 enzymes, *Chem. Rev. 104*, 3947−3980.

24. Schlichting, I., Berendzen, J., Chu, K., Stock, A. M., Maves, S. A., Benson, D. E., Sweet, R. M., Ringe, D., Petsko, G. A., and Sligar, S. G. (2000) The catalytic pathway of cytochrome P450cam at atomic resolution, *Science 287*, 1615−1622.

25. Grant, S. K., Green, B. G., Stiffey-Wilusz, J., Durette, P. L., Shah, S. K., and Kozarich, J. W. (1998) Structural requirements for human inducible nitric oxide synthase substrates and substrate analogue inhibitors, *Biochemistry 37*, 4174−4180.

26. Moali, C., Boucher, J. L., Sari, M. A., Stuehr, D. J., and Mansuy, D. (1998) Substrate specificity of NO synthases: detailed comparison of L-arginine, homo-L-arginine, their N$^\omega$-hydroxy derivatives, and N$^\omega$-hydroxynor-L-arginine, *Biochemistry 37*, 10453−10460.

27. Dijols, S., Perollier, C., Lefevre-Groboillot, D., Pethe, S., Attias, R., Boucher, J. L., Stuehr, D. J., and Mansuy, D. (2001) Oxidation of N$^\omega$-hydroxyarginine analogues by NO-synthase: the simple, non amino acid N-butyl N′-hydroxyguanidine is almost as efficient an NO precursor as N$^\omega$-hydroxyarginine, *J. Med. Chem. 44*, 3199−3202.

28. Jia, Q., Cai, T., Huang, M., Li, H., Xian, M., Poulos, T. L., and Wang, P. G. (2003) Isoform-selective substrates of nitric oxide synthase, *J. Med. Chem. 46*, 2271−2274.

29. Renodon-Corniere, A., Dijols, S., Perollier, C., Lefevre-Groboillot, D., Boucher, J. L., Attias, R., Sari, M. A., Stuehr, D., and Mansuy, D. (2002) N-Aryl N′-hydroxyguanidines, a new class of NO-donors after selective oxidation by nitric oxide synthases: structure−activity relationship, *J. Med. Chem. 45*, 944−954.

30. Xian, M., Fujiwara, N., Wen, Z., Cai, T., Kazuma, S., Janczuk, A. J., Tang, X., Telyatnikov, V. V., Zhang, Y., and Chen, X. (2002) Novel substrates for nitric oxide synthases, *Bioorg. Med. Chem. 10*, 3049−3055.

31. Fukuto, J. M., Wallace, G. C., Hszieh, R., and Chaudhuri, G. (1992) Chemical oxidation of *N*-hydroxyguanidine compounds. Release of nitric oxide, nitroxyl and possible relationship to the mechanism of biological nitric oxide generation, *Biochem. Pharmacol. 43*, 607−613.

32. Fukuto, J. M., Stuehr, D. J., Feldman, P. L., Bova, M. P., and Wong, P. (1993) Peracid oxidation of an *N*-hydroxyguanidine compound: a chemical model for the oxidation of N^ω-hydroxyl-L-arginine by nitric oxide synthase, *J. Med. Chem. 36*, 2666−2670.

33. Dijols, S., Boucher, J. L., Lepoivre, M., Lefevre-Groboillot, D., Moreau, M., Frapart, Y., Rekka, E., Meade, A. L., Stuehr, D. J., and Mansuy, D. (2002) First non-α-amino acid guanidines acting as efficient NO precursors upon oxidation by NO-synthase II or activated mouse macrophages, *Biochemistry 41*, 9286−9292.

34. Mueller, E. J., Loida, P. J., and Sligar, S. G. (1995) Twenty-five years of P450cam research, in *Cytochrome P450: Structure, Mechanism, and Biochemistry* (Ortiz de Montellano, P. R., Ed.) pp 83−124, Plenum Press, New York.

35. Rosen, G. M., Tsai, P., and Pou, S. (2002) Mechanism of free radical generation by nitric oxide synthase, *Chem. Rev. 102*, 1191−1199.

36. Porasuphatana, S., Tsai, P., and Rosen, G. M. (2003) The generation of free radicals by nitric oxide synthase, *Comp. Biochem. Physiol., Part C: Toxicol. Pharmacol. 134*, 281−289.

37. Presta, A., Siddhanta, U., Wu, C., Sennequier, N., Huang, L., Abu-Soud, H. M., Erzurum, S., and Stuehr, D. J. (1998) Comparative functioning of dihydro- and tetrahydropterins in supporting electron transfer, catalysis, and subunit dimerization in inducible nitric oxide synthase, *Biochemistry 37*, 298−310.

38. Bernatowicz, M. S., Wu, Y., and Matsueda, G. R. (1993) Urethane protected derivatives of 1-guanylpyrazole for the mild and efficient preparation of guanidines, *Tetrahedron Lett. 34*, 3389−3392.

39. Ghosh, S., Wolan, D., Adak, S., Crane, B. R., Kwon, N. S., Tainer, J. A., Getzoff, E. D., and Stuehr, D. J. (1999) Mutational analysis of the tetrahydrobiopterin-binding site in inducible nitric-oxide synthase, *J. Biol. Chem. 274*, 24100−24112.

40. Stuehr, D. J., and Ikeda-Saito, M. (1992) Spectral characterization of brain and macrophage nitric oxide synthases. Cytochrome P-450-like hemeproteins that contain a flavin semiquinone radical, *J. Biol. Chem. 267*, 20547−20550.

41. Wei, C. C., Wang, Z. Q., Durra, D., Hemann, C., Hille, R., Garcin, E., Getzoff, E. D., and Stuehr, D. J. (2005) The three nitric oxide synthases differ in their kinetics of tetrahydrobiopterin radical formation, heme-dioxy reduction, and arginine hydroxylation, *J. Biol. Chem. 280*, 8929−8935.

42. Marchal, S., Gorren, A. C., Sorlie, M., Andersson, K. K., Mayer, B., and Lange, R. (2004) Evidence of two distinct oxygen complexes of reduced endothelial nitric oxide synthase, *J. Biol. Chem. 279*, 19824−19831.

43. Wang, J., Stuehr, D. J., and Rousseau, D. L. (1997) Interactions between substrate analogues and heme ligands in nitric oxide synthase, *Biochemistry 36*, 4595−4606.

44. Tsubaki, M., Hiwatashi, A., and Ichikawa, Y. (1986) Effects of cholesterol and adrenodoxin binding on the heme moiety of cytochrome P-450$_{scc}$: a resonance Raman study, *Biochemistry 25*, 3563−3569.

45. Fan, B., Wang, J., Stuehr, D. J., and Rousseau, D. L. (1997) NO synthase isozymes have distinct substrate binding sites, *Biochemistry 36*, 12660−12665.

46. Li, D., Stuehr, D. J., Yeh, S. R., and Rousseau, D. L. (2004) Heme distortion modulated by ligand-protein interactions in inducible nitric-oxide synthase, *J. Biol. Chem. 279*, 26489−26499.

47. Spiro, T. G., and Wasbotten, I. H. (2005) CO as a vibrational probe of heme protein active sites, *J. Inorg. Biochem. 99*, 34−44.

48. Abu-Soud, H. M., Gachhui, R., Raushel, F. M., and Stuehr, D. J. (1997) The ferrous-dioxy complex of neuronal nitric oxide synthase. Divergent effects of L-arginine and tetrahydrobiopterin on its stability, *J. Biol. Chem. 272*, 17349−17353.

49. Sato, H., Sagami, I., Daff, S., and Shimizu, T. (1998) Autoxidation rates of neuronal nitric oxide synthase: effects of the substrates, inhibitors, and modulators, *Biochem. Biophys. Res. Commun. 253*, 845−849.

50. Lefevre-Groboillot, D., Boucher, J. L., Mansuy, D., and Stuehr, D. (2006) Reactivity of the heme-dioxygen complex of the inducible nitric oxide synthase in the presence of alternative substrates. *FEBS J. 273*, 180−191.

51. Wang, Z. Q., Wei, C. C., Ghosh, S., Meade, A. L., Hemann, C., Hille, R., and Stuehr, D. J. (2001) A conserved tryptophan in nitric oxide synthase regulates heme−dioxy reduction by tetrahydrobiopterin, *Biochemistry 40*, 12819−12825.

52. Spiro, T. G. (1985) Resonance Raman spectroscopy as a probe of heme protein structure and dynamics, *Adv. Protein Chem. 37*, 111−159.

53. Wells, A. V., Li, P., Champion, P. M., Martinis, S. A., and Sligar, S. G. (1992) Resonance Raman investigations of *Escherichia coli*-expressed *Pseudomonas putida* cytochrome P450 and P420, *Biochemistry 31*, 4384−4393.

54. Jung, C., Stuehr, D. J., and Ghosh, D. K. (2000) FT-Infrared spectroscopic studies of the iron ligand CO stretch mode of iNOS oxygenase domain: effect of arginine and tetrahydrobiopterin, *Biochemistry 39*, 10163−10171.

55. Stuehr, D., Pou, S., and Rosen, G. M. (2001) Oxygen reduction by nitric-oxide synthases, *J. Biol. Chem. 276*, 14533−14536.

56. Wang, Z. Q., Wei, C. C., and Stuehr, D. J. (2002) A conserved tryptophan 457 modulates the kinetics and extent of *N*-hydroxy-L-arginine oxidation by inducible nitric-oxide synthase, *J. Biol. Chem. 277*, 12830−12837.

57. Gorren, A. C., Bec, N., Schrammel, A., Werner, E. R., Lange, R., and Mayer, B. (2000) Low-temperature optical absorption spectra suggest a redox role for tetrahydrobiopterin in both steps of nitric oxide synthase catalysis, *Biochemistry 39*, 11763−11770.

58. Ray, G. B., Li, X.-Y., Ibers, J. A., Sessler, J. L., and Spiro, T. G. (1994) How far can proteins bend the FeCO unit? Distal polar and steric effects in heme proteins and models, *J. Am. Chem. Soc. 116*, 162−176.

59. Li, X.-Y., and Spiro, T. G. (1988) Is bound carbonyl linear or bent in heme proteins? Evidence from resonance Raman and infrared spectroscopic data, *J. Am. Chem. Soc. 110*, 6024−6033.

60. Migita, C. T., Salerno, J. C., Masters, B. S. S., Martasek, P., McMillan, K., and Ikeda-Saito, M. (1997) Substrate binding-induced changes in the EPR spectra of the ferrous nitric oxide complexes of neuronal nitric oxide synthase, *Biochemistry 36*, 10987−10992.

61. Proniewicz, L. M., and Kincaid, J. R. (1990) A Quantitative clarification of vibrationally coupled dioxygen in the resonance Raman spectra of cobalt-substituted heme proteins and model compounds, *J. Am. Chem. Soc. 112*, 675−681.

62. Jung, C., Schulze, H., and Deprez, E. (1996) Role of the polarity of the heme environment for the CO stretch modes in cytochrome P450cam-CO, *Biochemistry 35*, 15088−15094.

63. Li, T., Quillin, M. L., Phillips, G. N., Jr., and Olson, J. S. (1994) Structural determinants of the stretching frequency of CO bound to myoglobin, *Biochemistry 33*, 1433−1446.

64. Li, H., Shimizu, H., Flinspach, M., Jamal, J., Yang, W., Xian, M., Cai, T., Wen, E. Z., Jia, Q., Wang, P. G., and Poulos, T. L. (2002) The novel binding mode of *N*-alkyl-*N*′-hydroxyguanidine to neuronal nitric oxide synthase provides mechanistic insights into NO biosynthesis, *Biochemistry 41*, 13868−13875.

65. Raman, C. S., Li, H., Martasek, P., Southan, G., Masters, B. S. S., and Poulos, T. L. (2001) Crystal structure of nitric oxide synthase bound to nitro indazole reveals a novel inactivation mechanism, *Biochemistry 40*, 13448−13455.

66. Crane, B. R., Arvai, A. S., Ghosh, D. K., Wu, C., Getzoff, E. D., Stuehr, D. J., and Tainer, J. A. (1998) Structure of nitric oxide synthase oxygenase dimer with pterin and substrate, *Science 279*, 2121−2126.

67. Lefevre-Groboillot, D., Boucher, J. L., Stuehr, D., and Mansuy, D. (2005) Relationship between the structure of guanidines and *N*-hydroxyguanidines, their binding to inducible nitric oxide synthase (iNOS) and their iNOS-catalysed oxidation to NO, *FEBS J. 272*, 3172−3183.

68. Yamamoto, Y., and Kojima, S. (1991) *The Chemistry of Amidines and Imidates*, (Patai, S., and Rappoport, Z., Eds.) pp 485−526, John Wiley and Sons Inc., New York.

69. Harris, D. L., and Loew, G. H. (1998) Theoretical investigation of the proton assisted pathway to formation of cytochrome P450 compound I, *J. Am. Chem. Soc. 120*, 8941−8948.